
Combined radiofrequency ablation and doxorubicin-eluting polymer implants for liver cancer treatment

Brent D. Weinberg,¹ Elvin Blanco,² Scott F. Lempka,¹ James M. Anderson,³ Agata A. Exner,⁴ Jinming Gao²

¹Department of Biomedical Engineering, Case Western Reserve University, Cleveland, Ohio 44106

²Simmons Comprehensive Cancer Center, University of Texas Southwestern Medical Center, Dallas, Texas 75390

³Institute of Pathology, Case Western Reserve University, Cleveland, Ohio 44106

⁴Department of Radiology, Case Western Reserve University, Cleveland, Ohio 44106

Received 15 May 2006; accepted 19 May 2006

Published online 21 November 2006 in Wiley InterScience (www.interscience.wiley.com). DOI: 10.1002/jbm.a.30926

Abstract: Previously, biodegradable polymer implants (polymer millirods) to release chemotherapeutic agents directly into tumors have been developed. The purpose of this study is to evaluate local drug distribution from these implants in liver tumors treated with radiofrequency (RF) ablation and determine if the implants provide a therapeutic improvement over RF ablation alone. Cylindrical implants were fabricated using 65% poly(D,L-lactide-co-glycolide) (PLGA), 21.5% NaCl, and 13.5% doxorubicin. Control or drug-containing millirods were implanted inside VX2 liver tumors (11 mm diameter) in rabbits after RF ablation. Therapeutic efficacy was assessed 4 and 8 days after treatment using tumor size, histology, and fluorescence measurement of drug distribution. Tumors in both test groups recurred at the boundary of the ablated region. Therapeutic doxorubicin concentrations were found in

more than 80% of the ablated area, but concentrations declined rapidly at the boundary between normal and ablated tissue. This region was characterized by a developing fibrous capsule with resolving inflammation, which restricted drug transport out of the ablated zone. The intratumoral doxorubicin implants delivered high concentrations of drug within the ablated region but only limited amounts outside the ablation zone. Future studies will focus on overcoming the fibrotic transport barrier and enhancing drug delivery to the periphery of the ablation region to prevent tumor progression. © 2006 Wiley Periodicals, Inc. *J Biomed Mater Res* 81A: 205–213, 2007

Key words: biodegradable polymer; polymer implants; intratumoral drug delivery; VX2 tumor; minimally invasive therapy

INTRODUCTION

Minimally invasive cancer treatments have been a topic of much investigation in recent years. Many types of cancer, such as hepatocellular carcinoma, are difficult to treat surgically because of limited anatomical access or poor overall patient health.¹ Additionally, these cancers do not respond well to systemically administered chemotherapy, with patient response rates less than 30%.² With significant advances in image-guided technology, the ability to percutaneously administer treatments locally to tumors has improved dramatically. These percutaneous treatments have used a variety of ablative methods including ethanol³ or acetic acid injection⁴; heating

with radiofrequency (RF),⁵ laser,⁶ or microwave⁷ energy; and cryoablation.⁸ Among these, RF ablation has shown particular promise in treating liver disease because of high response rates and relatively low incidence of major side effects.⁹ However, tumor recurrence, particularly at the boundary of RF ablation, has been found as a major limitation of this treatment.¹⁰

Much research has attempted to improve the outcome of RF ablation for cancer treatment. One frequently employed strategy has been through technological improvement of ablation techniques aimed at achieving larger and more consistent treatment regions. These improvements, such as water-cooled tips, multitined electrodes, and saline injections prior to the procedure^{11,12} have led to overall increases in the size of tumors that can be successfully treated. An alternative adjuvant strategy used in animal and human trials has been the combination of RF ablation with chemotherapy. Several studies have shown increases in the size of treatment regions when combined with intravenous administration of liposomal doxorubicin.^{13,14} Furthermore, direct intratumoral

Correspondence to: J. Gao; e-mail: jinming.gao@utsouthwestern.edu

Contract grant sponsor: NIH; contract grant numbers: R01 CA090696, T32 GM07250

injections of liposomal doxorubicin have also shown benefit in the size and extent of ablation-treated tissue.¹⁰ A recent study demonstrated improved tumor treatment response from RF ablation followed by 5-FU impregnated polyanhydride implants compared to RF alone.¹⁵ These results underscore the potential for improving RF ablation by supplementing it with systemically or locally administered drugs.

As a means of providing locally controlled delivery of drugs to tumors after RF ablation, we have previously reported on the development of cylindrical polymer implants (polymer millirods) designed for use in conjunction with the ablation procedure.^{16–18} These implants were fabricated using poly(D,L-lactide-co-glycolide) (PLGA) and were manufactured to deliver several different chemotherapeutic agents, including 5-fluorouracil,¹⁹ carboplatin,²⁰ and doxorubicin.²¹ Their cylindrical design (diameter 1.6 mm; length 8–10 mm) was specifically tailored such that the implants could be delivered in a image-guided, minimally invasive fashion through the bore of a modified 14-gauge biopsy needle, which is already commonly used in image-guided biopsy procedures.²² Polymer millirods with different drug release kinetics have been developed, including rapid release (several days),¹⁸ sustained release (as many as 21 days),¹⁹ and dual-release (burst release followed by sustained release).²¹ Most recently, we demonstrated the antitumor effect of rapid release doxorubicin implants alone in treating small (8 mm diameter) VX2 liver tumors in rabbits.²³ Data showed that doxorubicin implants led to significant tumor shrinkage over drug-free implants; however, limited drug penetration distance (~2 mm) was not sufficient to adequately eliminate all VX2 tumor cells.

The goal of the current study is to determine whether combined treatment with RF ablation and drug implants improves treatment outcome over RF ablation alone. We chose a VX2 liver carcinoma model in New Zealand White rabbits for these studies. The tumors were first treated with purposely insufficient RF ablation to simulate incomplete treatment followed by the implantation of a doxorubicin-impregnated implant. Doxorubicin was used in the implants because of its previously reported success in combination with RF ablation^{13,14} and clinical use in liver cancer therapy.²⁴ The drug also has natural fluorescence, which allows for characterization of local drug distribution in tumor/liver tissues. In this study, we assessed tumor treatment four and eight days after the procedure by measuring gross tumor size, local drug distribution, and histology. Our hypothesis was that the doxorubicin-containing implants with RF ablation would facilitate drug retention and penetration inside tumor tissues, thereby increasing treatment efficacy over RF ablation or millirod therapy alone.

MATERIALS AND METHODS

Materials

Poly(D,L-lactide-co-glycolide) (PLGA, 1:1 lactide:glycolide, inherent viscosity 0.65 dL/g) was obtained from Birmingham Polymers (Birmingham, AL). Tris-buffered saline (TBS, pH 7.4), hydrochloric acid, sodium hydroxide, *N,N*-dimethylformamide (DMF), and dimethyl sulfoxide (DMSO) were purchased from Fisher Scientific (Pittsburg, PA). Methylene chloride, poly(vinyl alcohol) (MW 13,000–23,000 Da, 87–89% hydrolyzed), and Hank's balanced salt solution (HBSS) were acquired from Sigma-Aldrich (St. Louis, MO). Doxorubicin HCl (DOX) (2 mg/mL) in saline (9 mg/mL) was acquired from Bedford Laboratories (Bedford, OH). Teflon tubes (i.d. 1.6 mm) and stainless steel plungers (o.d. 1.6 mm) were purchased from McMaster-Carr Supply Company (Cleveland, OH). Fetal bovine serum (FBS) was obtained from Cambrex (East Rutherford, NJ).

Implant fabrication

Implants were produced by a compression molding procedure described previously.^{18,23} Briefly, PLGA microspheres (~4 μ m in diameter) were produced using a single-emulsion procedure. DOX in solution was concentrated by raising the pH to 9.0 with sodium hydroxide, washing with water, resuspending, and returning the solution pH to 3.0 with hydrochloric acid. The resulting concentrated solution was combined with doxorubicin in saline and lyophilized to yield a final powder containing 38.5% doxorubicin and 61.5% NaCl (w/w). To produce the implants, 65% PLGA microspheres, 21.5% NaCl, and 13.5% doxorubicin (w/w) were mixed with a mortar and pestle, packed into a Teflon tube, and compressed with steel plungers at 90°C for 2 h. Previous studies have shown that these implants release the majority of their doxorubicin loading *in vitro* within 24 h.²³ Control implants were produced using a similar procedure with 100% PLGA.

Animals and tumor model

Adult New Zealand White rabbits ($n = 16$; Covance, Princeton, NJ) weighing 2.8–3.2 kg were used. Studies with these animals were approved by the Institutional Animal Care and Use Committee at Case Western Reserve University and carried out according to its guidelines. All surgical procedures were performed under intramuscular anesthesia with ketamine (40 mg/kg), acetylpromazine (5 mg/kg), and xylazine (5 mg/kg).

The tumor model used in this study was the VX2 carcinoma in rabbit liver, which has been widely used in studies of minimally-invasive and image-guided procedures.^{25,26} VX2 cells were first grown for 4 weeks in the thigh muscle of a donor rabbit. This tumor was harvested, cut into small pieces 1.5 mm on each side, and frozen in FBS containing 10% DMSO in a liquid nitrogen storage tank. Before implantation, the tumor pieces were thawed and washed three times in HBSS. Liver tumors were generated in the livers of

the study rabbits by implanting a small piece of frozen tumor tissue in the rabbit liver. The abdomen of the recipient rabbit was shaved and a midline incision just distal to the sternum was made. The anterior surface of the middle liver lobe was perforated to a depth of 5 mm with the outer cannula of a 22-gauge angiocatheter, and a piece of tumor measuring approximately 1 mm³ was placed into the puncture. The tumor piece was secured in place with a small piece of gelatin foam and a single biodegradable suture. The tumors were then allowed to grow in the liver for 18 days until they reached an approximate diameter of 11 mm.

Tumor treatment procedure

All tumors were treated with RF ablation, and rabbits were randomly assigned to two groups. Control group subjects ($n = 8$) received a drug-free implant, and treatment group subjects ($n = 8$) received a doxorubicin-containing implant after RF ablation was performed. For treatment, the abdomen was opened and the liver tumor located by palpation. A 17-gauge, 1 cm exposed tip ablation probe (Radionics, Burlington, MA) was inserted into the center of the tumor perpendicular to the surface of the liver. The tumor tissue was then ablated to a temperature of 80°C for 2 min, a condition sufficient to create an ablated region approximately 8 mm in diameter. Following ablation, a control or doxorubicin-containing millirod was placed into the electrode tract and secured again using a small piece of gelatin foam and a single suture. Half of the animals in each group were euthanized with a barbiturate overdose at 4 and 8 days after the treatment. Doxorubicin content remaining in the implants was measured by dissolving the implant in 2 mL DMF and extracting the remaining doxorubicin.¹⁷ The solution was diluted to 20 mL with TBS and centrifuged to remove precipitated polymer. Doxorubicin concentration of the solution was then determined by measuring the absorption at 480 nm on a spectrophotometer (Perkin Elmer Lambda 20).

Tumor analysis

Tumors were removed from the surrounding liver tissue and sliced in half at an orientation perpendicular to the implant track. The halves of the tumor were photographed, and one half of the tumor was placed in 10% buffered formalin solution, while the other half of the tumor was frozen at -20°C. The fixed tissue was embedded in paraffin, sliced, and stained with hematoxylin and eosin (H&E), or Masson's trichrome (MTC). Unstained sections were analyzed qualitatively with fluorescence microscopy. Maps of the entire stained histology slices at 40× magnification were generated at using a video microscopy system consisting of a light microscope (Olympus BX60), video camera (Sony DXC-390), position encoded motorized stage (Prior Scientific ProScan), and software (Media Cybernetics Image-Pro).²⁷ Ablated tissue, viable tumor, and inflammatory regions on these image maps were identified and manually segmented using the ImageJ (NIH) software.

Quantitative fluorescence analysis

We modified a previously established fluorescent imaging technique for measuring the fluorescent doxorubicin in tissue slices²⁸ to include subtraction of an ablated tissue background. Frozen tissue samples were sliced to 100- μ m thick sections on a cryostat microtome (Microm 505E) and scanned with a fluorescent imager (Molecular Dynamics Fluorimager SI) with the following conditions: pixel size, 100 μ m; bit depth, 16; photomultiplier gain, 850; and high sensitivity mode. An average ablation background was generated from slices of the control-treated tumors because the fluorescence of the ablated tissue varied with distance from the ablation probe. Each point within the ablated region was assigned a location between 0 and 1, according to its relative distance between the ablation center and the ablated/normal tissue interface. Fluorescence values were binned and averaged by their location to obtain a curve of background fluorescence as a function of distance from the ablation center. For each treated tissue slice, every point within the ablation was similarly assigned a location based on the fractional distance between the ablation center and ablation boundary, and the net fluorescence intensity (NFI) was calculated by subtracting the background value that corresponded to that location. NFI was converted to doxorubicin concentration using a previously published equation, $NFI = 194 \cdot [Dox]^{0.67}$, where [Dox] is the doxorubicin concentration in μ g/g.²³ This empirical equation was acquired by imaging weighed slices of liver containing known quantities of doxorubicin. Average drug distribution profiles were calculated by finding the mean of 4 profiles evenly spaced by 90° around the fluorescence image. Values were binned in increments of 0.2 mm to decrease noise. The drug penetration distance was calculated as the average distance between the implant boundary and the point where the drug concentration dropped below 64 μ g/g, which is 10 times the therapeutic drug concentration.^{29,30} To estimate the total mass of drug remaining in the tumor, we determined the average drug concentration within 4 mm of the implant surface (the approximate size of the ablated area) and multiplied this value by the tissue volume.

RESULTS

Tumor treatment results

VX2 tumors were implanted in the middle liver lobe of 16 rabbits, 8 each in the control and treatment categories. At the time of treatment, one animal in the day 4 control group did not appear to have a tumor. In a second animal in the day 8 treatment group, the tumor was significantly adhered to the lateral peritoneal wall such that the tumor could not be safely ablated. These subjects were excluded from further study. The remaining 14 rabbits had tumors in the middle lobe that were treated with RF ablation followed by the implantation of a drug-free or doxorubicin-containing implant. A summary of the treatment outcomes is shown in Table I. Livers

TABLE I
Summary of Tumor Treatment Outcome after RF Ablation and Implantation
of a Drug-Free or Doxorubicin-Containing Millirod

		Livers with Viable Tumor	Ablation Area (cm ²)	Inflammatory Area (cm ²)	Residual Tumor Area (cm ²)
Day 4	Control	1/3	0.89 ± 0.54	0.29 ± 0.04	0.89
	Treatment	2/4	0.71 ± 0.30	0.15 ± 0.14	2.11, 0.75
Day 8	Control	1/4	0.81 ± 0.31	0.23 ± 0.10	0.57
	Treatment	0/3	0.82 ± 0.28	0.21 ± 0.07	n/a

All values are shown as ± Standard Deviation.

with viable tumor were found in 3 out of the 4 treatment groups. The presence of residual tumor cells in these livers was confirmed by histology. Viable tumor was not detected in any of the rabbits in the day 8 treatment group. Grossly, the treated tissues were all characterized by a single, spherical region of ablated tissue. Livers with residual cancer contained tumor nodules outside the region of ablation-induced necrosis.

Tumor histology

Tissue histology was used to further assess the outcome of different treatment groups. Typical images of H&E-stained tissue section from an RF ablated liver on day 8 are shown in Figure 1. Figure 1(A) is a low magnification overview of the entire treated region, showing the ablation-treated region (dashed line), outside of which are two nodes of recurrent tumor (asterisks). A lighter staining region characterized by a moderate inflammatory response, infiltrating fibroblasts, and mild collagen deposition was found to circumscribe the ablation-treated region. The ablated region shows typical coagulative necrosis from RF ablation, and a greater magnification of this region is illustrated in Figure 1(B). The outlines of pretreated cells are somewhat visible, but most cytoplasmic and nuclear details are lost. Necrotic debris and partially staining cells are contained throughout the area. In contrast, the tumor region outside the ablated zone shown in Figure 1(C) is filled with viable tumor cells, which appear relatively unaffected by the nearby ablation 8 days before. The cells in this region have all of the common characteristics of VX2 cells: dense packing, low differentiation, high nuclear to cytoplasm ratio, and the presence of mitotic figures. This pattern of recurrence, a treated region bounded by untreated areas of tumor, was found in all of the liver samples with incompletely treated tumors.

Closer inspection of the doxorubicin-treated slides is shown in Figure 2. MTC-stained images are shown alongside fluorescent microscopy images from the same region. In the MTC stain on day 4 [Fig. 2(A)], the boundary between ablated and normal tissue is subtle and characterized by the presence of

inflammatory cells. Fluorescence from that region [Fig. 2(B)] shows doxorubicin fluorescence that gradually tapers across the ablation boundary. In contrast, by day 8 [Fig. 2(C)], the boundary has become much more evident and is clearly demarcated by a blue-staining boundary approximately 200 μm thick, showing moderate collagen deposition. The corresponding fluorescent image [Fig. 2(D)] shows doxorubicin in the ablated region that drops off abruptly at the ablation boundary.

Region quantification

To further quantify the effects of ablation alone and the combined treatment, areas of ablation necrosis, inflammatory tissue, and, when present, viable tumor, were calculated using regions of interest manually segmented on histology. The results are shown in Table I. The mean sizes of all 14 ablated regions and inflammatory regions were 0.80 ± 0.32 and 0.22 ± 0.10 cm², respectively. There were no statistically significant differences found between any of the groups. The individual areas of recurrent tumors are also shown in the table, but again, no major differences between groups are readily apparent. From the tumor images, it was also possible to calculate distances from the ablation center. In the day 4 tumors receiving RF ablation followed by doxorubicin-containing implants, the two residual tumors began on average 4.1 mm from the ablation electrode location, 50% of tumor was found within 7.9 mm, and 100% of the tumor area was within 12.0 mm. These distances provide valuable information about what drug distribution would be necessary to limit tumor regrowth.

Drug release in vivo

Several values quantifying drug release *in vivo* are shown in Table II. Doxorubicin masses in the original implant, the extracted implant, and in the surrounding tissue as measured by fluorescence are shown along with the values as a percentage of the original doxorubicin loading. After 4 and 8 days, an insignificant amount of drug remained in the im-

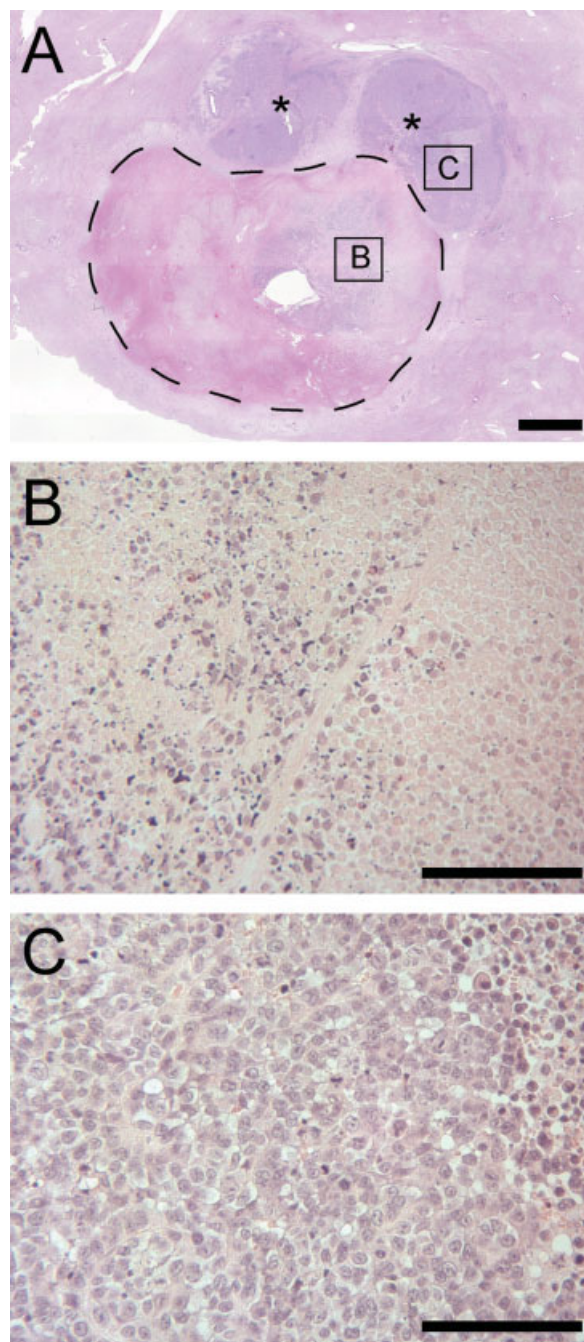


Figure 1. Representative H&E histology of tumor progression after RF ablation in a day 8 control subject. A: Overview of tumor region showing ablation treatment boundary (dashed line), two nodules of viable tumor (*), and regions magnified below. B: High magnification image of ablation-treated necrotic region. C: High magnification region of viable tumor cells untreated by the ablation. Scale bars are 2 mm in (A) and 200 μm in (B) and (C). [Color figure can be viewed in the online issue, which is available at www.interscience.wiley.com.]

plants. The drug penetration distances, defined as the average distance from the implant at which the drug concentration dropped below 64 $\mu\text{g/g}$, were 3.7 mm on day 4 and 2.1 mm on day 8. In addition

to critical drug concentrations being found 1.6 mm further from the implant on day 4, the tissue on day 4 retained significantly more of the original drug (20.4% of loading) than tissue on day 8 (3.8%). Apparent elimination rate from the tumor tissue and local half life were determined by fitting a decaying exponential of the form $D(t) = D_0 \exp(-kt)$ to the known drug masses in tissue. The elimination rate from the tumor area was $k = 0.35 \pm 0.02 \text{ day}^{-1}$ and apparent elimination half-time from tumor was of $t_{1/2} = 2.0 \pm 0.1 \text{ days}$.

Local drug distribution

Fluorescent imaging of tissue slices from the tumors revealed local drug concentrations in the extracted tissue. Two-dimensional doxorubicin distribution maps from these tissue sections are shown in Figure 3. Slices perpendicular to the long axis of the implant as well as parallel to the implant are shown for day 4 and day 8. Drug concentrations on day 4 exceed 2,000 $\mu\text{g/g}$ and extend completely to the ablation boundary [Fig. 3(A)]. Day 8 tissue drug concentrations are characterized by lower drug concentrations ($\sim 1,000 \mu\text{g/g}$) and a different distribution pattern [Fig. 3(C)]. This pattern consists of two regions of high drug concentration, within 2 mm of the implant boundary and a ring at the periphery of the ablated region, separated by a cleared zone containing much less drug. Slices parallel to the long axis of the implant show drug concentrations radiating from the flat end of the cylindrical implant on day 4 [Fig. 3(B)] and day 8 [Fig. 3(D)]. These distributions have similar properties but feature slightly lower drug concentrations and a less conspicuous clearing between the implant and the ablation boundary. The drug does not accumulate substantially beyond the ablation boundary.

Drug distribution profiles

To quantitatively display the drug distribution data, drug concentrations were binned and averaged in 0.2 mm increments for all animals from each time point. The resulting radial distribution profiles are shown as a function of the implant boundary in Figure 4. The figure numerically corroborates the observations from the 2D drug distributions. Drug concentrations are significantly higher on day 4, where significant amounts of drug extend roughly to the ablation boundary found at approximately 4 mm. On day 8, average concentrations dip to near 0 by 2 mm, but rise again slightly from drug observed at the ablation boundary. On average, significant

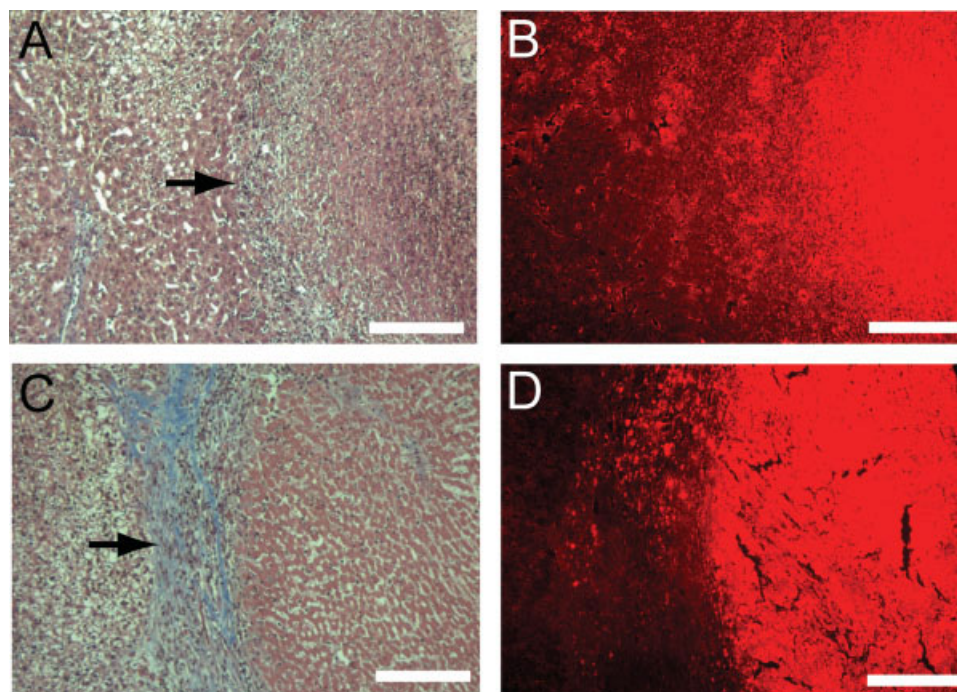


Figure 2. MTC-stained images of the ablation boundary on day 4 (A) and day 8 (C). Fluorescent microscopy images of the matching regions on day 4 (B) and day 8 (D). Ablated tissue is on the right and normal tissue on the left of each slide, with the boundary marked by the black arrows. Scale bars are 200 μm . [Color figure can be viewed in the online issue, which is available at www.interscience.wiley.com.]

amounts of doxorubicin do not extend beyond the ablation boundary.

DISCUSSION

In this study, tumors were treated by RF ablation supplemented with doxorubicin-containing PLGA implants. Local drug distributions were monitored, and therapeutic efficacy was compared against tumor treatment with RF ablation alone. Previous studies have shown that intratumorally administered drugs have a maximum effect on enlarging the treatment area when administered within 30 min after ablation,

with much of the effect lost after 48 h.¹⁰ The rapid-releasing implants used in this study seek to maximize tumor drug exposure during the narrow time window of drug sensitivity while minimizing the risk of drug resistance, which could occur if tumor cells were treated with drug concentrations below the therapeutic level for long periods of time. To simulate a clinical situation in which ablation incompletely treats cells at the tumor periphery, VX2 tumors in rabbit liver were treated with an ablation intensity not expected to completely eradicate the tumors.

Measurements of local doxorubicin concentrations around the implants revealed elevated drug concentrations in the ablation-treated region throughout the study. On day 4, more than 80% of the ablation coa-

TABLE II
Summary of Millirod Implant and Drug Release Properties

Drug Release Characteristics	Day 4	Day 8
Original drug loading (μg)	2990 \pm 200	3080 \pm 120
Drug remaining in extracted implant (μg)	190 \pm 50	200 \pm 30
Drug released (μg)	2800 \pm 200	2880 \pm 90
Drug released (% of original loading)	93.7 \pm 1.6	93.6 \pm 0.8
Drug in tissue (μg)*	590 \pm 300	120 \pm 100
Drug in tissue (% of original loading)*	20.4 \pm 11.6	3.8 \pm 3.0
Drug penetration distance (mm)*	3.7 \pm 1.3	2.1 \pm 0.3
Ablation region with [DOX] > 64 $\mu\text{g/g}$ (% of area)	81.4 \pm 13.8	39.9 \pm 28.1

Percentages shown are based on the original drug loading. All values are shown as \pm Standard Deviation.

* p -value of <0.1.

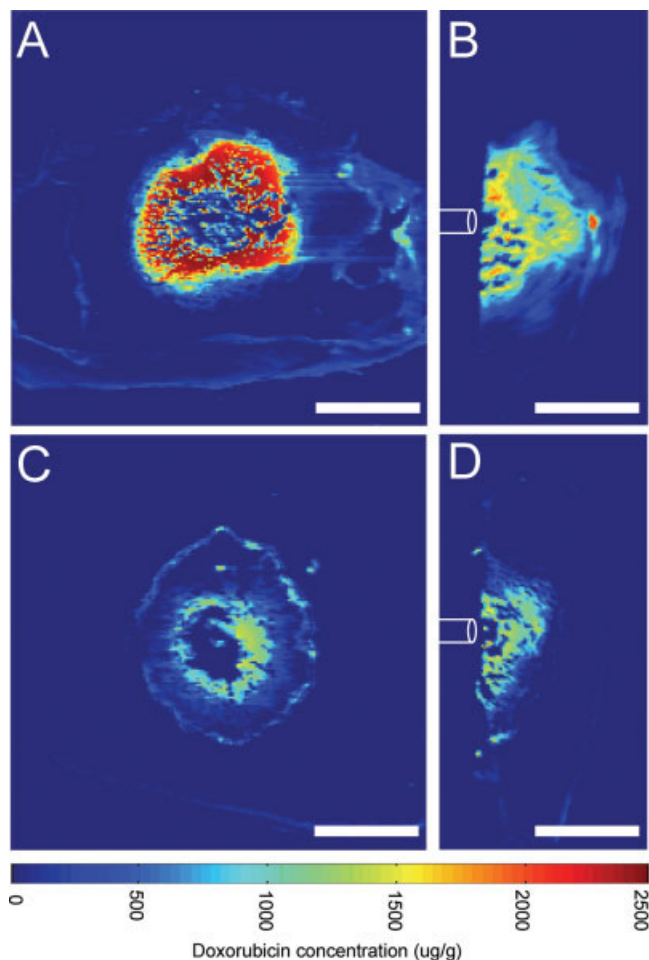


Figure 3. Doxorubicin concentration distribution maps from fluorescent imaging. Day 4 slices through the tumor center perpendicular to the implant axis (A) and slices through the end of the tumor parallel to the implant (B). Corresponding slices through the center of the tumor (C) and the end of the tumor (D) on day 8. The white cylindrical outlines indicate the approximate orientation of the implants in the parallel slices before removal. Scale bars are 5 mm. [Color figure can be viewed in the online issue, which is available at www.interscience.wiley.com.]

gulated zone contained drug at concentrations greater than $64 \mu\text{g/g}$, or 10 times higher than the accepted therapeutic concentration. Although this coverage dropped to 40% by day 8, drug concentrations as high as $1,000 \mu\text{g/g}$ were still seen adjacent to the implant and just inside the ablation boundary. Ablation of the tumor tissue facilitated the spread of drug from the implants, as the doxorubicin penetration distance (3.7 mm) and total doxorubicin contained in the tumor (20.4%) at day 4 were substantially higher than values previously reported for nonablated tumors (2.8 mm, 6.3%).²³ Furthermore, the apparent elimination half-life from ablated tumor (2.0 ± 0.1 days) is longer than previously found in nonablated tumors (1.6 ± 0.2 days), indicating that drug is eliminated more slowly from ablated tumor

than from normal tumor.²³ This may arise because ablation destroys tumor vasculature, halts mechanisms for drug metabolism, and increases drug binding to macromolecules.¹⁶ These data demonstrate the advantage of using RF ablation to improve drug delivery efficiency from millirod implants inside VX2 tumors. Meanwhile, despite high drug concentrations within the ablated area, concentrations dropped steeply to undetectable levels outside the ablation boundary. Viable tumor cells were found beyond the ablation boundary in both groups on day 4 (1/3 control vs. 2/4 treatment) but only in the control group on day 8 (1/4 control vs. 0/3 treatment). While the results represent a possible improvement in the day 8 treatment group, concluding that the treatment is better than the control is limited by small group sizes and experimental variability among rabbits.

Detailed results from histological analysis of the treated tissue sections provide insight about possible limitations of this treatment strategy. Tumors recurred outside the ablation area, where doxorubicin was not seen in substantial amounts at either time point. Doxorubicin transport to the cells outside the ablated region was limited by the formation of an inflammatory region around the ablated tissue. At day 4 this boundary consisted largely of neutrophils and monocytes typical of the chronic stages of inflammation, but by day 8 the boundary contained predominantly fibroblasts and moderate collagen deposition characteristic of fibrous capsule formation. Formation of this boundary has been previously noted in ablated normal liver tissue, where it was noted as a potential barrier to drug transport.³¹ The inflammatory tissue may act as a transport barrier in two ways. First, fibrous capsule formation with collagen deposition may create a boundary that is denser and more tortuous than ablated tumor or normal liver, which

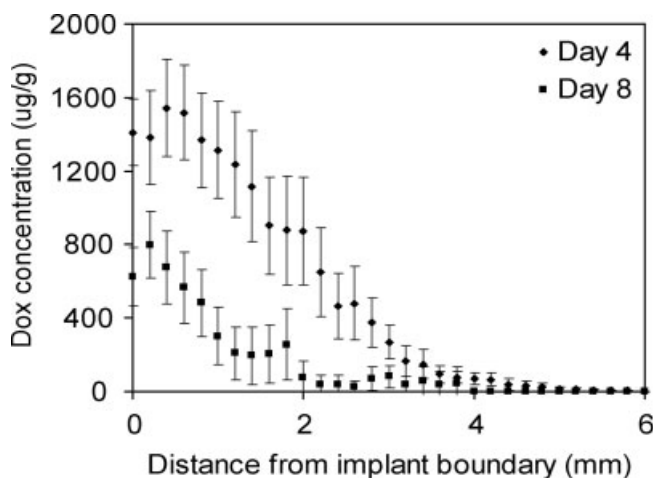


Figure 4. Average doxorubicin concentration plotted against distance from the implant boundary for day 4 and day 8. Error bars represent the 95% confidence interval.

may result in slower diffusion through this area. Second, the boundary may have a higher rate of drug clearance and metabolism due to a high fraction of vascular tissue and large number of cells that may take up and metabolize drugs and debris. A combination of these two effects limited drug exposure outside the ablation boundary, where tumor cells were found at distances ranging from 3.5 to 10.9 mm away from the implant location.

Overall, the potential benefit of combined therapy using RF ablation and chemotherapeutic implants is high despite some challenges. Doxorubicin infiltrated the tumor tissue to a greater distance and was retained in the tissue to a greater extent than when these implants were used in tumors without ablation.²³ Drug concentrations throughout the ablated region exceeded therapeutic values throughout the 8-day study period. On the other hand, untreated tumor cells persisted outside the ablated area, where drug was not found in substantial quantities. Identifying the role of fibrous capsule development in restricting doxorubicin delivery to tumor cells beyond the periphery of the ablated region is a key finding of this study. Future attempts at combining RF ablation with drug releasing implants must consider this challenge in their design.

Several improvements to the combined treatment strategy could maximize the therapeutic efficacy of these implants. Previous work has found that implants that sustain their drug release over several days provide greater drug coverage and penetration distances.¹⁷ However, since the fibrous boundary becomes progressively denser and less permeable to drug released at a later time, sustained drug release might not improve the treatment outcomes. Three other alternative strategies could overcome the fibrous boundary and improve treatment effectiveness. First, incorporation of an anti-inflammatory drug such as dexamethasone has been shown to markedly reduce the formation of the fibrous capsule after ablation³² and could be incorporated along with an anticancer drug such as doxorubicin. Second, alternative implant placements closer to the periphery of the ablated zone could reduce the drug transport distance to the viable tumor cells. Third, concurrent administration of systemic therapy targeted to the tumor periphery, such as nanoparticles targeted to tumor vasculature, may more effectively deliver drugs to the tumor cells most likely to survive ablation. Each of these approaches could maximize the therapeutic impact of local implants for tumor treatment in future studies.

CONCLUSIONS

This paper describes the use of RF ablation followed by doxorubicin-containing PLGA implants to

treat liver tumors. Despite the presence of therapeutic doxorubicin concentrations in the majority of the ablated region, tumors recurred around the boundary of the ablated zone where little drug was found. The distance of residual tumor from the implant and the extensive transport barrier posed by fibrous capsule formation after ablation restricted drug transport beyond the ablated region, thereby limiting treatment effectiveness. Nonetheless, the potential clinical benefits of implants for use in combined treatments are significant and future improvements to implant design and treatment strategies could lead to more ideal treatment.

BW is supported in part by DOD predoctoral fellowship BC043453.

References

1. Leung TW, Johnson PJ. Systemic therapy for hepatocellular carcinoma. *Semin Oncol* 2001;28:514–520.
2. Little SA, Fong Y. Hepatocellular carcinoma: Current surgical management. *Semin Oncol* 2001;28:474–486.
3. Livraghi T, Benedini V, Lazzaroni S, Meloni F, Torzilli G, Vettori C. Long term results of single session percutaneous ethanol injection in patients with large hepatocellular carcinoma. *Cancer* 1998;83:48–57.
4. Shah SS, Jacobs DL, Krasinkas AM, Furth EE, Itkin M, Clark TW. Percutaneous ablation of VX2 carcinoma-induced liver tumors with use of ethanol versus acetic acid: Pilot study in a rabbit model. *J Vasc Interv Radiol* 2004;15:63–67.
5. Goldberg SN. Radiofrequency tumor ablation: Principles and techniques. *Eur J Ultrasound* 2001;13:129–147.
6. Vogl TJ, Mack MG, Muller PK, Straub R, Engelmann K, Eichler K. Interventional MR: Interstitial therapy. *Eur Radiol* 1999;9:1479–1487.
7. Ohmoto K, Tsuduki M, Shibata N, Takesue M, Kunieda T, Yamamoto S. Percutaneous microwave coagulation therapy for hepatocellular carcinoma located on the surface of the liver. *AJR Am J Roentgenol* 1999;173:1231–1233.
8. Garcea G, Lloyd TD, Aylott C, Maddern G, Berry DP. The emergent role of focal liver ablation techniques in the treatment of primary and secondary liver tumours. *Eur J Cancer* 2003;39:2150–2164.
9. Barnett CC Jr, Curley SA. Ablative techniques for hepatocellular carcinoma. *Semin Oncol* 2001;28:487–496.
10. Goldberg SN, Saldinger PF, Gazelle GS, Huertas JC, Stuart KE, Jacobs T, Kruskal JB. Percutaneous tumor ablation: Increased necrosis with combined radio-frequency ablation and intratumoral doxorubicin injection in a rat breast tumor model. *Radiology* 2001;220:420–427.
11. Buscarini E, Buscarini L. Radiofrequency thermal ablation with expandable needle of focal liver malignancies: complication report. *Eur Radiol* 2004;14:31–37.
12. Livraghi T, Goldberg SN, Monti F, Bizzini A, Lazzaroni S, Meloni F, Pellicano S, Solbiati L, Gazelle GS. Saline-enhanced radio-frequency tissue ablation in the treatment of liver metastases. *Radiology* 1997;202:205–210.
13. Ahmed M, Liu Z, Lukyanov AN, Signoretti S, Horkan C, Monsky WL, Torchilin VP, Goldberg SN. Combination radio-frequency ablation with intratumoral liposomal doxorubicin: Effect on drug accumulation and coagulation in multiple tissues and tumor types in animals. *Radiology* 2005;235:469–477.

14. Ahmed M, Monsky WE, Girmun G, Lukyanov A, D'Ippolito G, Kruskal JB, Stuart KE, Torchilin VP, Goldberg SN. Radiofrequency thermal ablation sharply increases intratumoral liposomal doxorubicin accumulation and tumor coagulation. *Cancer Res* 2003;63:6327–6333.
15. Haaga JR, Exner AA, Wang Y, Stowe NT, Tarcha PJ. Combined tumor therapy by using radiofrequency ablation and 5-FU-laden polymer implants: Evaluation in rats and rabbits. *Radiology* 2005;237:911–918.
16. Qian F, Stowe N, Liu EH, Saidel GM, Gao J. Quantification of in vivo doxorubicin transport from PLGA millirods in thermoablated rat livers. *J Control Release* 2003;91:157–166.
17. Qian F, Stowe N, Saidel GM, Gao J. Comparison of doxorubicin concentration profiles in radiofrequency-ablated rat livers from sustained- and dual-release PLGA millirods. *Pharm Res* 2004;21:394–399.
18. Qian F, Szymanski A, Gao JM. Fabrication and characterization of controlled release poly(D,L-lactide-co-glycolide) millirods. *J Biomed Mater Res* 2001;55:512–522.
19. Qian F, Nasongkla N, Gao JM. Membrane-encased polymer millirods for sustained release of 5-fluorouracil. *J Biomed Mater Res* 2002;61:203–211.
20. Szymanski-Exner A, Gallacher A, Stowe NT, Weinberg B, Haaga JR, Gao J. Local carboplatin delivery and tissue distribution in livers after radiofrequency ablation. *J Biomed Mater Res A* 2003;67:510–516.
21. Qian F, Saidel GM, Sutton DM, Exner A, Gao JM. Combined modeling and experimental approach for the development of dual-release polymer millirods. *J Control Release* 2002;83:427–435.
22. Daniel BL, Birdwell RL, Butts K, Nowels KW, Ikeda DM, Heiss SG, Cooper CR, Jeffrey SS, Dirbas FM, Herfkens RJ. Freehand iMRI-guided large-gauge core needle biopsy: A new minimally invasive technique for diagnosis of enhancing breast lesions. *J Magn Reson Imaging* 2001;13:896–902.
23. Weinberg BD, Ai H, Blanco E, Anderson JM, Gao J. Antitumor efficacy and local distribution of doxorubicin via intratumoral delivery from polymer millirods. *J Biomed Mater Res A*. Forthcoming.
24. Leung TW, Patt YZ, Lau WY, Ho SK, Yu SC, Chan AT, Mok TS, Yeo W, Liew CT, Leung NW, Tang AM, Johnson PJ. Complete pathological remission is possible with systemic combination chemotherapy for inoperable hepatocellular carcinoma. *Clin Cancer Res* 1999;5:1676–1681.
25. Hazle JD, Stafford RJ, Price RE. Magnetic resonance imaging-guided focused ultrasound thermal therapy in experimental animal models: correlation of ablation volumes with pathology in rabbit muscle and VX2 tumors. *J Magn Reson Imaging* 2002;15:185–194.
26. Miao Y, Ni Y, Mulier S, Yu J, De Wever I, Penninckx F, Baert AL, Marchal G. Treatment of VX2 liver tumor in rabbits with “wet” electrode mediated radio-frequency ablation. *Eur Radiol* 2000;10:188–194.
27. Breen MS, Lazebnik RS, Wilson DL. Three-dimensional registration of magnetic resonance image data to histological sections with model-based evaluation. *Ann Biomed Eng* 2005;33:1100–1112.
28. Gao JM, Qian F, Szymanski-Exner A, Stowe N, Haaga J. In vivo drug distribution dynamics in thermoablated and normal rabbit livers from biodegradable polymers. *J Biomed Mater Res* 2002;62:308–314.
29. Ridge JA, Collin C, Bading JR, Hancock C, Conti PS, Daly JM, Raaf JH. Increased adriamycin levels in hepatic implants of rabbit Vx-2 carcinoma from regional infusion. *Cancer Res* 1988;48:4584–4587.
30. Swistel AJ, Bading JR, Raaf JH. Intraarterial versus intravenous adriamycin in the rabbit Vx-2 tumor system. *Cancer* 1984;53:1397–1404.
31. Blanco E, Qian F, Weinberg B, Stowe N, Anderson JM, Gao J. Effect of fibrous capsule formation on doxorubicin distribution in radiofrequency ablated rat livers. *J Biomed Mater Res A* 2004;69:398–406.
32. Blanco E, Weinberg BD, Stowe NT, Anderson JM, Gao J. Local release of dexamethasone from polymer millirods effectively prevents fibrosis after radiofrequency ablation. *J Biomed Mater Res A* 2006;76:174–182.